WELDING RESEARCH

SUPPLEMENT TO THE *WELDING JOURNAL*, JUNE 1995
Sponsored by the American Welding Society and the Welding Research Council

Acoustic Emission Investigation of Cold Cracking in Gas Metal Arc Welding of AISI 4340 Steel

Theoretical models fit reasonably well with experimental data in using acoustic emmission signals to detect cold cracks

BY C.-K. FANG, E. KANNATEY-ASIBU, JR., AND J. R. BARBER

ABSTRACT. Acoustic emission (AE) has been used to investigate the propagation of a finite crack in a weldment subjected to nonuniform longitudinal residual stresses during gas metal arc welding (GMAW). Cold cracking in selected weldments was accelerated using the electrochemical method to cathodically charge the weldments with hydrogen in order to induce hydrogen embrittlement. Cold cracking was observed about 40 min after charging in the specimen subjected to hydrogen embrittlement, while it was observed two days after welding for the one that was left in the atmosphere. The AE signals were generated as the specimen cracked and were recorded, and the effects from structure and instrumentation were removed from the measured signals by deconvolution in the frequency domain. Most of the high-amplitude signal components were found to be clustered in the frequency range below 200 kHz. The experimentally obtained spectrum was compared with theoretical results derived in earlier work, and reasonable agreement with theoretical surface displacement in both time and frequency domains was obtained. The envelopes for both spectra were found to decrease with increasing frequency, while the fluctuations in each curve diminished at high frequencies.

C.-K. FANG, E. KANNATEY-ASIBU, JR., and J. R. BARBER are with the Department of Mechanical Engineering and Applied Mechanics, University of Michigan, Ann Arbor, Mich.

KEY WORDS

Acoustic Emission
Cold Cracking
Residual Stress
GMAW
AISI 4340 Steel
Crack Propagation
Hydrogen Embrittlement
Frequency Range
Time Domain
Theoretical Simulation

Introduction

Welding processes are often associated with discontinuities caused either by improper welding conditions or disturbances that change the preset conditions. Cracking is the most damaging of all the discontinuities in weldments. Cracks could be formed either during welding (*i.e.*, soon after solidification), which is hot cracking, or after the bead has cooled to room temperature. This latter, which is cold cracking, may continue for several hours, days, weeks, or even months. Cold cracking or delayed cracking, as it is sometimes called, is the focus of this research.

Due to the intense heat input in welding, significant variations in physical and chemical properties occur, which in turn lead to changes of microstructure (*e.g.*, martensitic transformation) in the heat-affected zone (HAZ), especially for high-hardenability steels. These often cause a decrease in the fracture toughness of the material, which, coupled with the residual stress due to solidification and thermal shrinkage, and sometimes hydrogen embrittlement for high-strength steels, may result in cracking. Several techniques have been developed for detecting weldment cracks, but acoustic emission (AE) has been found to be more suited to real-time monitoring.

Acoustic emission is a transient elastic wave generated by the rapid release of energy within a material (Ref. 1). It is generated while the phenomenon is undergoing change, and is therefore highly suitable for real-time or continuous monitoring. The AE technique has been applied to the on-line monitoring of a variety of manufacturing processes, *e.g.*, casting (Refs. 2, 3), machining (Refs. 4, 5) and welding (Ref. 6). In the detection of cold cracking in weldments, it has been studied by a number of researchers (Refs. 7–10). The AE spectrum from cracking

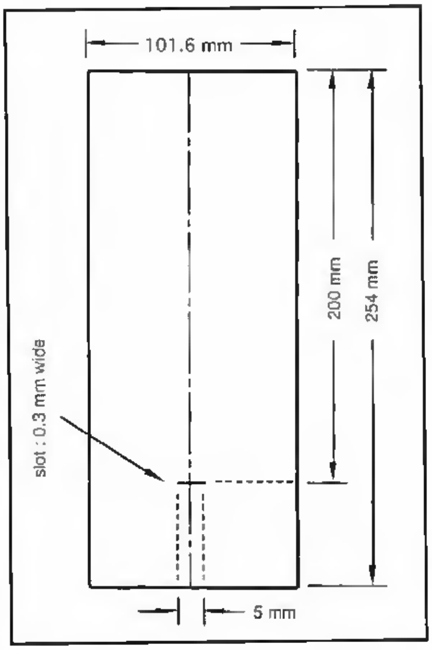

Fig. 1 — Specimen configuration and dimensions.

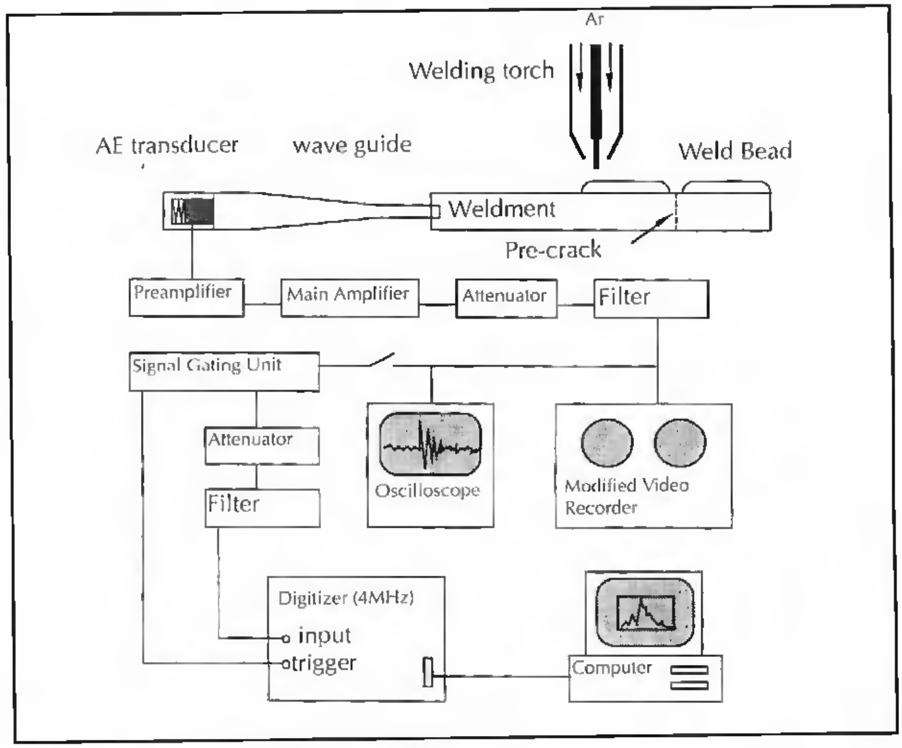

Fig. 2 — Acoustic emission monitoring system.

has been studied by Graham and Alers (Ref. 11), Ono and Ucisik (Ref. 12), and Honjoh, *et al.* (Ref. 13). Liu and Kannatey-Asibu, Jr., (Ref. 6) used the AE spectrum as features in the pattern-recognition analysis of defects in welding. More physical insight might be helpful in the interpretation of the AE spectrum and in turn improve the pattern recognition ability. Very little, however, has been done to correlate experimental spectra with theoretical modeling, especially for AE from the propagation of a finite crack under nonuniform residual stresses in a weldment.

Experimental work is undertaken in this paper for comparison with a theoretical analysis of surface motion due to propagation of a finite crack in a weldment subjected to nonuniform residual stresses (Ref. 14). The latter involves the growth of transverse through cracks in weldments. All welding was done using gas metal arc welding. To facilitate the generation of cracks, we considered the four principal factors essential for producing cold cracks, *viz.*, brittle structure; high stresses; the presence of hydrogen; and low temperatures (Ref. 15). For a brittle structure, we used a high hardenability material (AISI 4340 alloy steel), with high cooling rates induced by a liquid nitrogen quench to promote the formation of the brittle phase. Cracking was induced by hydrogen embrittlement, which was accelerated by the electrochemical method through cathodic charging of the specimens with hydrogen. Thus, no external loading was needed to crack the specimen, and the residual stress distribution was maintained. The AE signals from cracking were recorded and transformed into the frequency domain. We note that the observed AE spectrum is significantly influenced by the resonance and transmission characteristics of both the structure (geometry and acoustic properties) and the instrumentation (Ref. 16). These effects were removed from the measured signals by deconvolution in the frequency domain. The spectrum was then correlated with the theoretically obtained surface motion.

Experimental Procedure

Specimen Preparation

A commercially available AISI 4340 high-strength steel was selected because of its high hardenability and susceptibility to cold cracking. Its chemical composition was 0.41% C, 0.75% Mn, 0.008% P, 0.003% S, 0.23% Si, 1.75% Ni, 0.82% Cr, 0.13% Cu, 0.25% Mo, and the balance Fe, with an as-received hardness of 196 BHN. Three plates (marked No. 1, No. 2, and No. 3) with dimensions 254 x 101.6 x 9.5 mm (10 x 4 x 0.37 in.) were used in the experiments.

In order to introduce a crack configuration similar to the one analyzed theoretically in the previous work (Ref. 14., *i.e.*, a transverse through crack across the weld centerline), the specimen was precracked using electrical discharge machining (EDM) before welding. The location of the precrack was selected so that the distance between the AE sensor and source met the far-field requirement (Ref. 14). As shown in Fig. 1, the precrack was a through slot of length 5 mm (0.2 in.) and a width of 0.3 mm (0.01 in.) in a direction perpendicular to the weld centerline. The theoretical results were based on the assumption that the crack propagates in a uniform medium. However, the HAZ of the as-welded specimen is mainly composed of martensite, whose fracture toughness is significantly lower than that of the base metal. In order to introduce the brittle phase (martensite) in the base metal region, also, each specimen was austenitized at 850°C (1562°F) for 30 min and then quenched in water before welding. No quench cracking was observed. To avoid melting at the precracked region during welding, the slot was masked using high-temperature cement before welding.

AE System Setup

Each specimen was monitored by an acoustic emission system during and after welding. The schematic diagram of the AE system setup is illustrated in Fig. 2. A differential acoustic emission transducer was used. It was calibrated using the ASTM Standard E1106. Figure 3

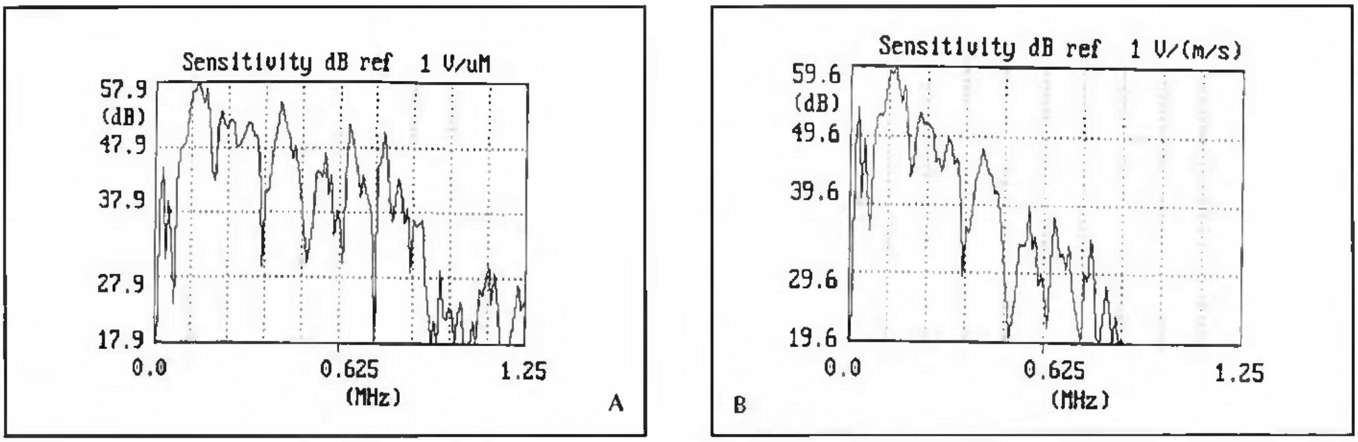

Fig. 3 — Sensitivities of the transducer to: A — surface displacement; B — surface velocity.

shows the sensitivities of the transducer to: a) surface displacement; and b) surface velocity. Since the former has a more uniform frequency response than the latter (with a cut-off frequency of 875 kHz), we expect that the output voltage depends more on the surface displacement. In order to isolate the transducer from thermal shock, a waveguide 11.5 in. (292 mm) long was attached by threading to the far end parallel to the slot of each plate. The distance between the center of the slot and the attachment was 200 mm (7.8 in.). The transducer was spring loaded against the other end of the waveguide and acoustically coupled with commercially available AE couplant.

The transducer was connected to a preamplifier with 40 dB gain and 20 kHz high-pass filter, followed by a main amplifier with an adjustable gain. The signal from the main amplifier then goes to a filter, and the upper cut-off frequency was set at 1 MHz. The signals were then recorded using a modified video recorder with a 2-MHz bandwidth. Because the amplitude of the signal produced by cracking is relatively high, and the recorder would saturate for voltages exceeding the operation range of –1 to 1 V, the signals were attenuated by 20 dB before recording to avoid saturation. An oscilloscope was used to monitor the signals.

Welding Experiment

After setting up the AE system, bead-on-plate welds were then produced using a computer-controlled gas metal arc welding machine using argon (Ar) shielding. A commercial AWS ER 70S-6 electrode of 1.6 mm (0.062 in.) in diameter was utilized as a welding wire, which contains 0.07–0.15C, 1.40–1.85Mn, 0.80–1.15Si, 0.02P, 0.02S, and the balance Fe. The constant voltage mode with reverse polarity (electrode positive) was used. The welding conditions, including average arc voltage and current of 31.4 V and 389.5 A, respectively, and a travel speed of 7.5 mm/s (17.7 in./min), were used. Other welding conditions were wire feed rate 4 m/min (157 in./min), and welding time 16 s. Only specimen No. 1 was restrained at the four corners by parallel clamps, while the other specimens were free of external restraint. In each specimen, welding was started from a location 5 mm (0.2 in.) from the edge parallel and closest to the slot, and was continued for a length of 130 mm (5 in.), with the weld bead perpendicular to the slot. Liquid nitrogen was poured on the specimen immediately after welding to induce martensitic transformation. The cement was then removed and the area around the slot sanded and rinsed using acetone.

System Calibration

Before cold cracking, each specimen was calibrated together with the setup. A 3H pencil lead of 3 mm (0.1 in.) length and 0.3 mm (0.01 in.) diameter was used, to which a quasi-statically increasing force was applied, in the vertical direction and at the crack center, until fracture occurred. Three calibration signals were recorded for each specimen, and their average in the frequency domain was taken.

Hydrogen Embrittlement

Specimen No. 1 was not subjected to

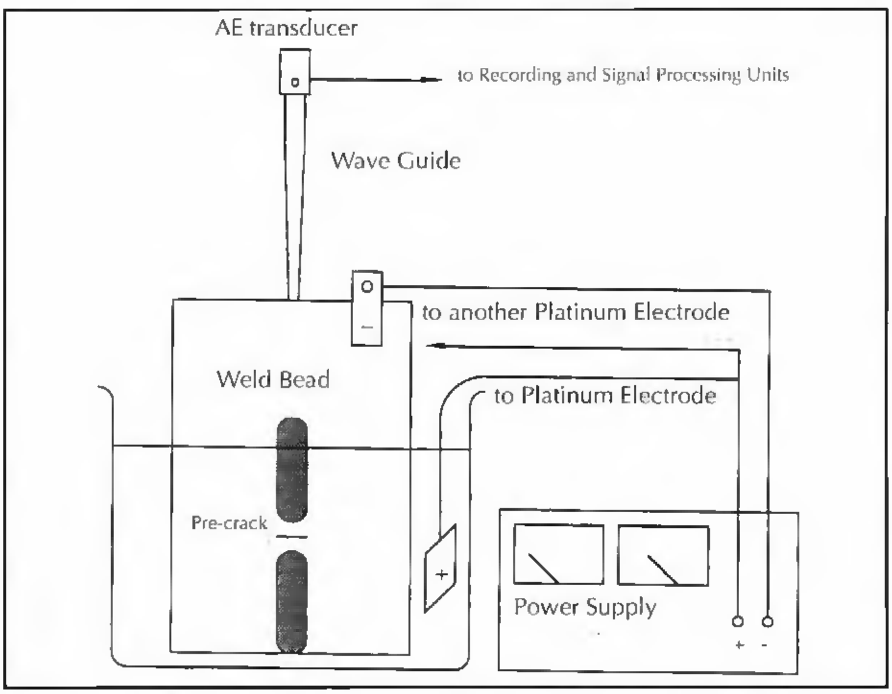

Fig. 4 — Experimental setup for hydrogen charging using electrochemical method.

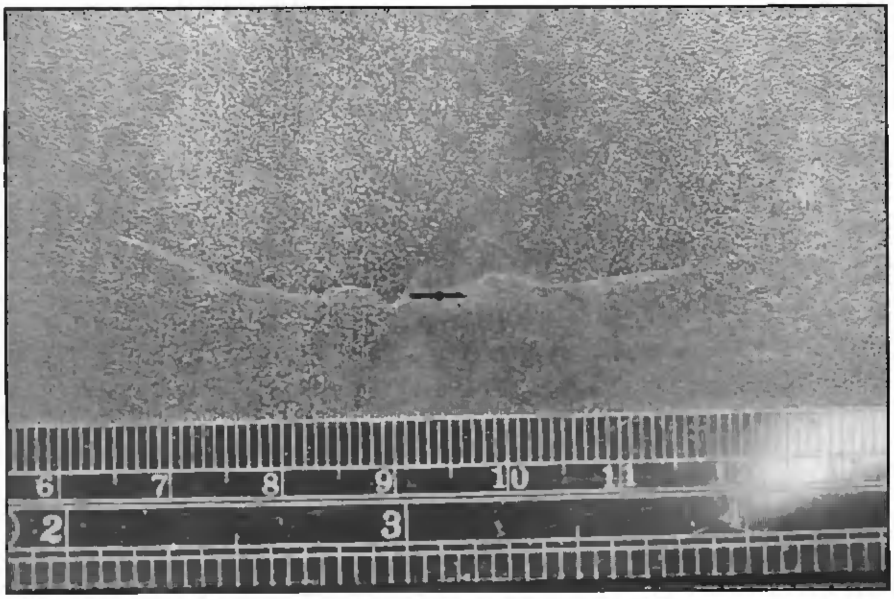

Fig. 5 — Photograph of delayed crack in atmosphere.

hydrogen charging. Hydrogen embrittlement was induced in the other two specimens (Nos. 2, 3) using the electrochemical method. The experimental conditions for specimens Nos. 2 and 3 were the same for checking reproducibility. In order to restrict cracking to the neighborhood of the slot, the surfaces of specimens Nos. 2 and 3 were masked, except for the region around the slot with an area of 40 x 5 mm (1.6 x 0.2 in.), on both sides. Weldments Nos. 2 and 3 were then individually immersed in an 800 mL, 1N sulfuric acid (H_2SO_4) electrolyte and connected to the negative port of a DC power supply, as shown in Fig. 4. The anodes (counter electrodes) were two platinum sheets with dimensions 25.4 x 25.4 x 0.0254 mm (1 x 1 x 0.0001 in.) each. They were immersed in the solution on both sides of the plate to ensure uniform current density. Specimens Nos. 2 and 3 were then individually charged with hydrogen at constant current density (100 mA/cm^2) in the solution, to which 11.5 mg arsenic trioxide (As_2O_3) had been added to prevent the combination of the absorbed atomic hydrogen into molecular hydrogen.

Signal Conditioning

The calibration signals and those from cracking were recorded and subsequently played back for analysis. On playback, the recorder was put in a pause mode at the desired location of the tape. The output analog signal was passed through a signal gating unit, through which a 16.7 ms length of the signal was clipped for sampling. It was then digitized with a 0.25 μs sampling period. To avoid saturation of the digitizer, which has an operating range of –256 to 256 mV, an attenuator was installed before it. The signal from the digitizer was then fed to a computer for data analysis in both time and frequency domains.

Results and Discussion

During and immediately after welding and quenching, a lot of AE burst signals were observed. These may have been due to microcracking in the weldment. The AE from microcracking is not of major concern in this research. Instead, we are more interested in the propagation of finite cracks, which can be compared with the simulation based on earlier analysis (Ref. 14).

The first specimen (No. 1) cracked about two days after welding. A photograph of the finite crack on the lower side of the specimen is shown in Fig. 5. The corresponding AE signal was not obtained because the recorder could only record signals over a period of one hour. This was the reason for using hydrogen charging to accelerate the cracking for the other two specimens (Nos. 2 and 3).

Specimen Nos. 2 and 3 showed good reproducibility in the experiments. The cracking for these two specimens occurred about 40 min after hydrogen charging in the electrolyte. The photograph in Fig. 6 depicts the crack on the lower surface of specimen No. 2. The crack lengths were 64 mm (2.5 in.) and 64.5 mm (2.54 in.) on the upper and lower sides, respectively, for specimen No. 2. They were 62 mm (2.4 in.) and 64 mm for specimen No. 3.

No AE signals were observed before and after the burst from the crack propagation during hydrogen charging. This is quite different from the results of Ohira and Pao (Ref. 17), and of Ohira and Kishi (Ref. 18), where an A533B and an Al-Zn-Mg-Cu alloy were tested, respectively. They found that the large-amplitude AE was preceded by several small-amplitude AE signals. They postulated that the small-amplitude AE signals were produced by the nucleation of voids (microcracks) around the main crack, presumably from the decohesion of inclusions of MnS in steels, while the large-amplitude AE is attributed to the growth of the main crack, which was observed when the stress intensity factor exceeded the fracture toughness. Since no such small-amplitude AE signals were observed prior to

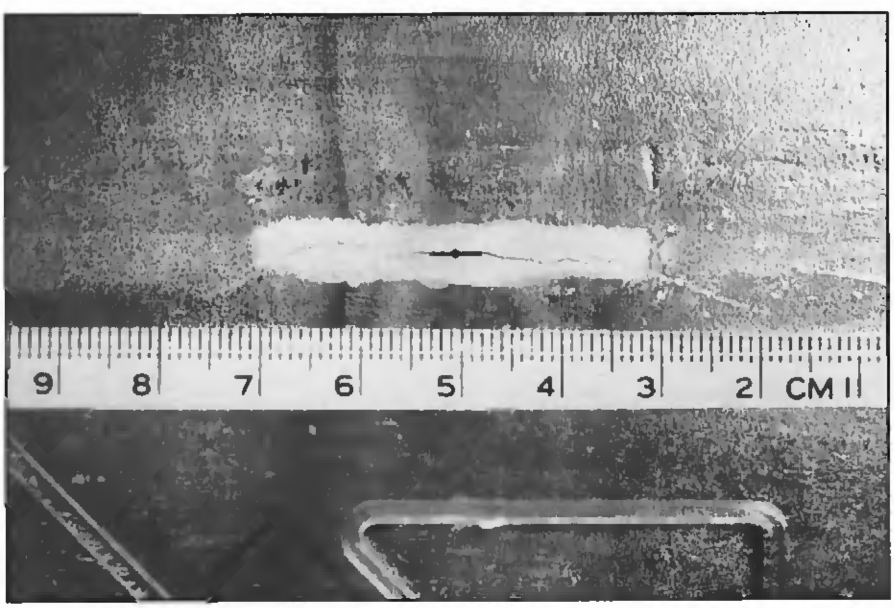

Fig. 6 —Photograph of delayed crack after hydrogen charging in electrolyte.

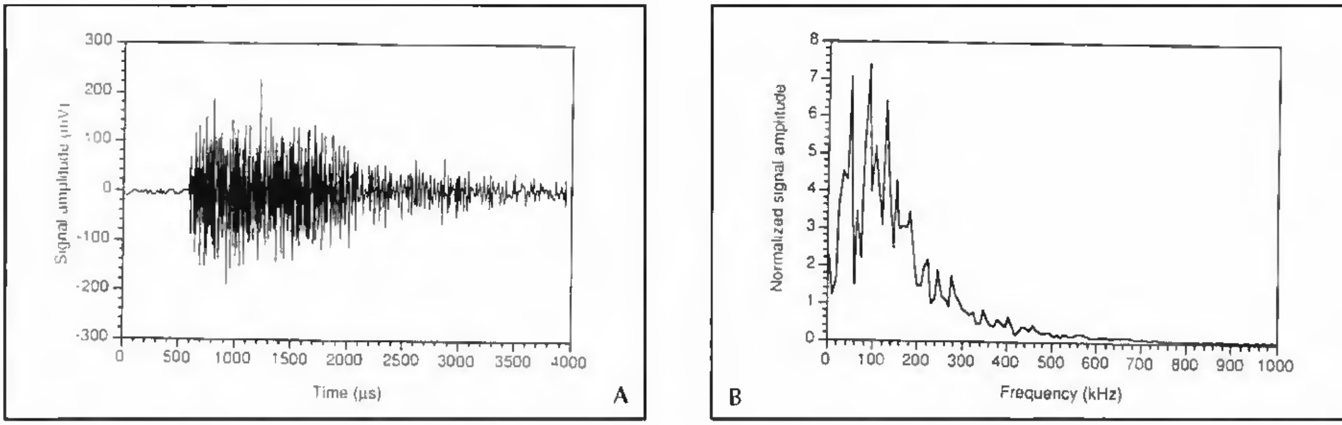

Fig. 7 — A — Acoustic emission signal from crack propagation; B — frequency response of cracking signal (the amplitude has been normalized by the mean).

the burst in our observation, there must be no "initiation, growth, and coalescence of microvoid," a ductile failure, in our test. This is due to the fact that our test essentially involved brittle fracture because of the nitrogen quenching and hydrogen embrittlement of the specimen.

The time domain AE signal due to cracking and its corresponding spectrum are shown in Fig. 7. Each spectrum in this work was normalized by the mean amplitude. The amplitude in Fig. 7A has been adjusted by the attenuator to accommodate the voltage range of the digitizer, *i.e.*, between −256 and 256 mV. The attenuation was 0.27. The later portion of the signal in the time domain is due to oscillation of the transducer and the propagation within the structure due to multiple reflections of the stress waves. As can be seen in Fig. 7B, the spectrum is concentrated in the frequency range below 200 kHz. This is consistent with the Graham and Alers (Ref. 11) experimental AES spectrum analysis in tensile tests for A533-B pressure vessel steel. They found that the AES associated with cracking were characterized by having frequency components predominantly below 200 kHz.

The signal shown in Fig. 7 includes the characteristics of the structure and instrumentation. To get rid of these effects, a deconvolution of the signal using the calibration signal is necessary. The time and frequency domain AE responses due to pencil lead breakage are shown in Fig. 8. The spectrum shown in Fig. 8B was the average of three calibration signals.

The pencil lead breakage can give a well-defined point unloading step-function force (Ref. 19) with a 1 µs rise time and 4–5 N load release for 2H pencil lead of 0.5 mm diameter (Ref. 20). Since the rise time can be reduced by increasing the hardness (or brittleness) and decreasing the diameter of the pencil lead (Ref. 21), it should be less than 1 µs for the pencil lead used in this experiment (3H, and 0.3 mm in diameter). Consequently, the source function of the pencil lead breakage can be approximated by a step function given by $S_p(t) = FH(t)$, where F is the force magnitude, and H(t) the Heaviside unit step function of time. Alternatively, it can be expressed as $S_p(\omega) = F/(i\omega)$ in the frequency domain, where ω is the circular frequency and $i = \sqrt{-1}$. If the AE spectrum due to pencil lead breakage, as shown in Fig. 8, is represented by $E_p(\omega)$, the transfer function $G(\omega)$ of the entire system (including the specimen, waveguide and instrumentation) can be obtained by deconvolution in the frequency domain, giving $G(\omega) = E_p(\omega)/S_p(\omega) = i\omega E_p(\omega)/F$. Now $G\omega$ is the AE frequency response due to a vertical impulse force acting at the location of the AE source. It carries the information on characteristics of the instrumentation and propagation within the structure due to multiple reflections and mode conversions. The spectrum of $G(\omega)$ is illustrated in Fig. 9.

Once the transfer function of the system is available, we can remove the effects of structure and instrumentation from the measured cracking signals, $E_c(\omega)$, by deconvolution in the frequency domain. The result, is $E_c(\omega)/G(\omega)$, shown in Fig. 10, where the amplitude has been normalized by the mean. As can be seen in the spectrum, most of the high-amplitude components are clustered at frequencies below 200 kHz, while the high-frequency components are relatively small. This is in agreement with the state

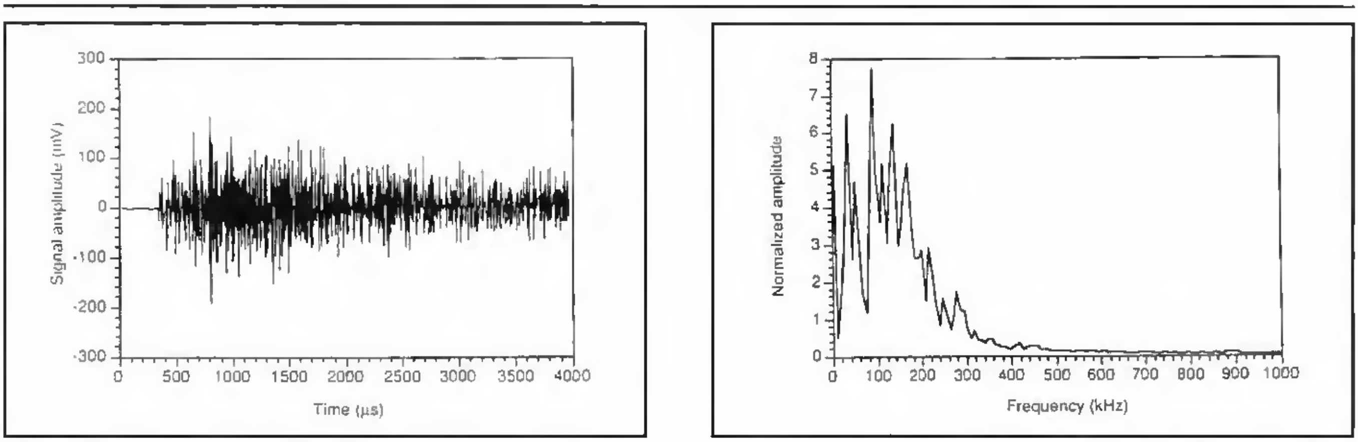

Fig. 8 — A — Time domain acoustic emission signal of pencil lead breakage for calibration at the crack center; B — frequency response of calibration signal (the amplitude has been normalized by the mean).

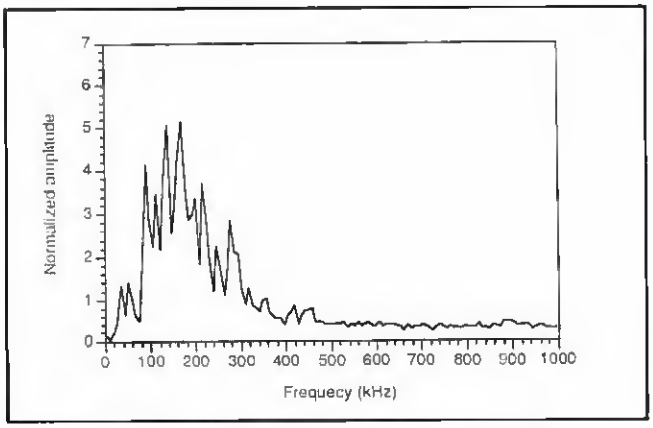

Fig. 9 — System transfer function in the frequency domain.

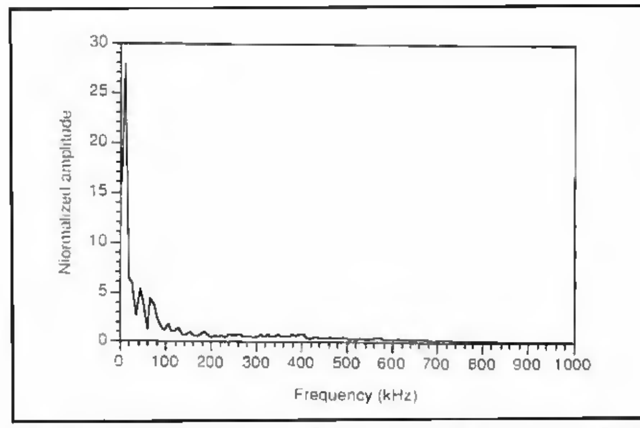

Fig. 10 — Experimental spectrum of cracking after deconvolution (the amplitude for each spectrum has been normalized by the mean).

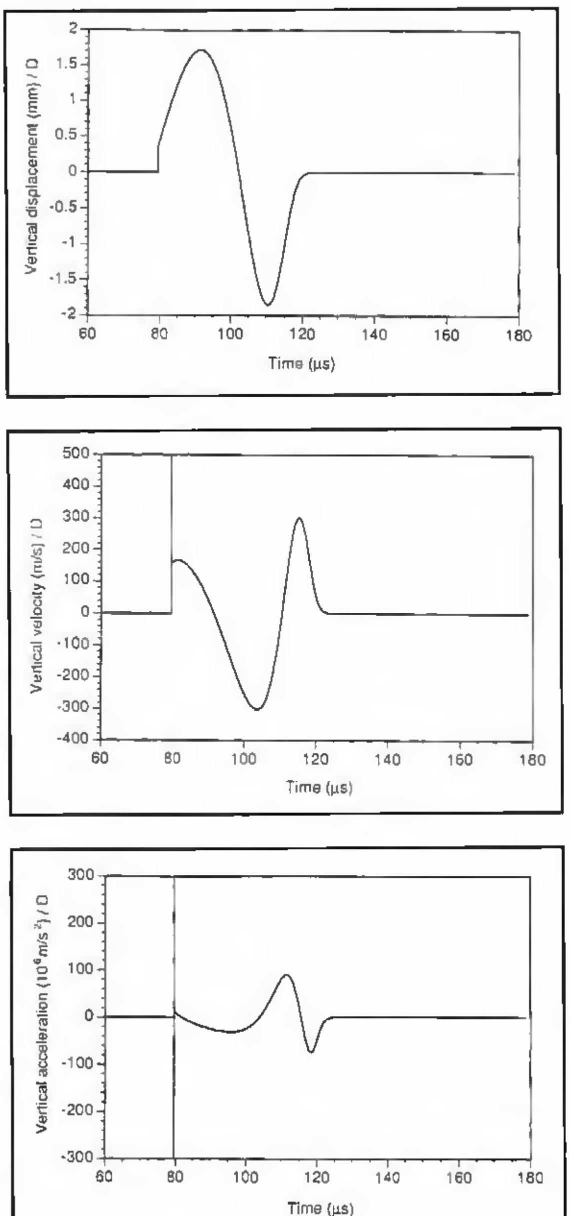

Fig. 11 — Theoretical surface motion at the epicenter. A — Vertical displacement; B — vertical velocity; and C — vertical acceleration.

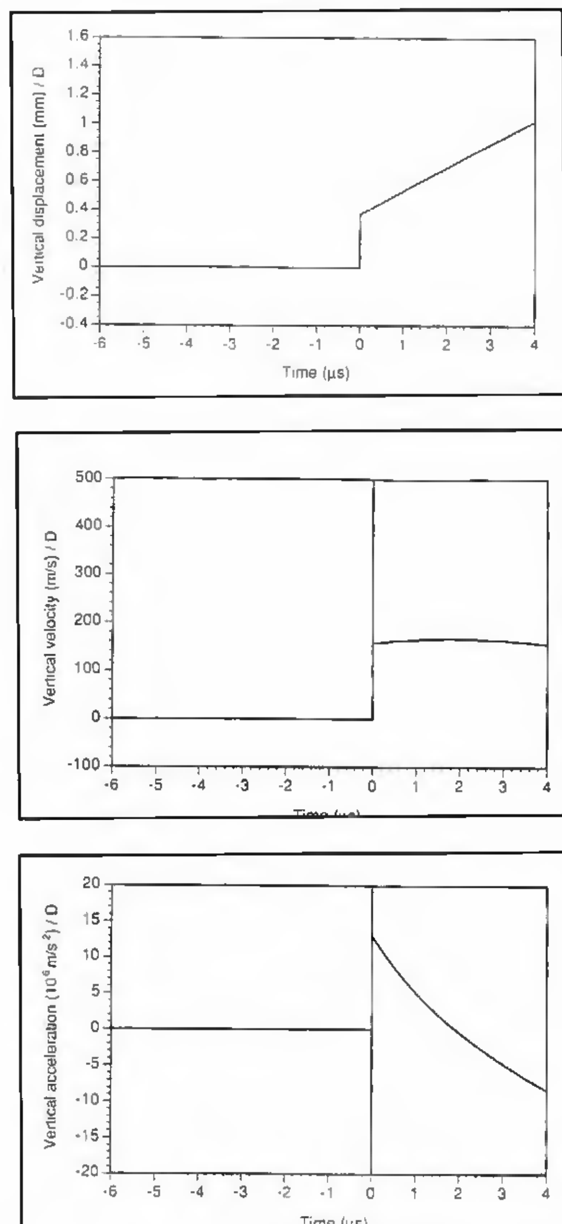

Fig. 12 — Theoretical initial response. A — vertical displacement; B — Vertical velocity; C — vertical acceleration.

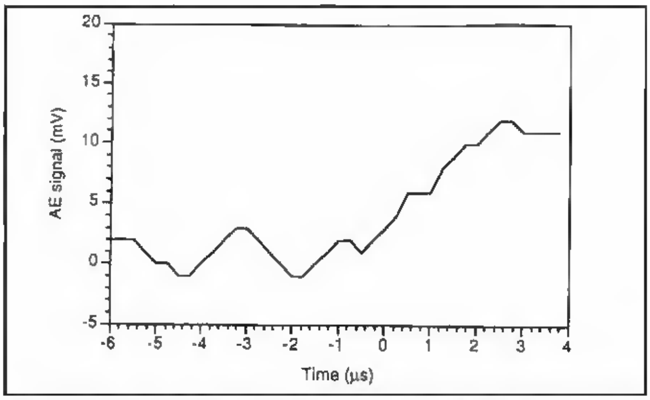

Fig. 13 — Theoretical spectra of vertical motion at the epicenter (the amplitude has been normalized by the mean of each curve).

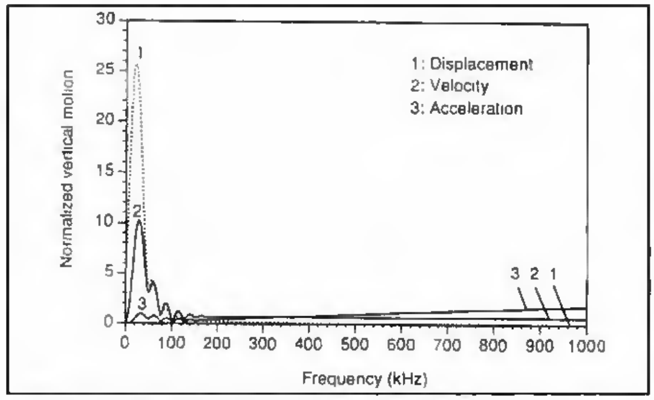

Fig. 14 — Theoretical spectra of vertical motion at the epicenter (the amplitude has been normalized by the mean of each curve).

ment of Spanner, *et al.* (Ref. 16), that the single most common frequency range for acoustic emission testing is 100 to 300 kHz.

To compare the experimental spectrum with theoretical prediction, we substitute experimental parameters into the theoretical results obtained in the previous work (Ref. 14), where the vertical displacement at the epicenter of a weldment subjected to a nonuniform residual stress was derived as:

$$u_v(x_2,t) = D\frac{v\left(t-\frac{x_2}{C_d}\right)}{C_d}\left[a\left(t-\frac{x_2}{C_d}\right)-\frac{3a^3\left(t-\frac{x_2}{C_d}\right)}{4c^2}\right] \quad (1)$$

where x_2 is the distance between the source and sensor, C_d is the longitudinal stress wave speed, a and v are instantaneous crack length and speed, respectively, c is the half width of the longitudinal residual stress tension zone, and D is a dimensionless constant which remains fixed for a given set of experimental conditions.

The instantaneous crack length, a, in Equation 1 can be simulated using the crack-tip equation of motion (Ref. 22):

$$\frac{1-\frac{1}{C_R}\frac{da}{dt}}{\sqrt{1-\frac{1}{C_d}\frac{da}{dt}}}\left\{1-\left[\frac{1}{v_c}\frac{da}{dt}\right]^n\right\}= \left[\frac{K_{IM}}{K_{IO}}\right]\frac{f(a_o/c)}{f(a/c)}\sqrt{\frac{a_o}{\eta_b a}} \quad (2)$$

where

$$f(a/c)=\int_0^{a/c}\left[1-\zeta^2\right]\exp\left[-\frac{\zeta^2}{2}\right]\frac{1}{\sqrt{(a/c)^2-\zeta^2}}d\zeta \quad (3)$$

and $\zeta = \xi_1/c$. Here, C_R is the Rayleigh wave speed, v_c is the limiting crack speed, K_{IO} and K_{IM} are the fracture toughness for crack initiation and arrest, respectively, n is the shape factor of the dynamic fracture toughness vs. crack speed curve, and η_b is the bluntness parameter of the crack tip. The experimental parameters are: initial crack half length a_o = 2.5 mm, x_2 = 492 mm, K_{IO} = 61 MPa $m^{1/2}$, K_{IM} = 52 MPa $m^{1/2}$, C_d = 6201 m/s, C_R = 3217 m/s, V_c = 1250 m/s, and n = 1.75 for AISI 4340 steel (Ref. 22). Two more parameters, η_b and c, need to be evaluated before performing the simulation. The bluntness parameter η_b of the precrack can be determined from the root radius of the slot, which is 0.15 mm (0.006 in.). According to the blunt notch testing results of 4340 steel given by Datta (Ref. 23), the apparent fracture toughness K_{IO}' for a notch with a root radius 0.15 mm is about 2.74 times larger than the initiation fracture toughness K_{IO} for a sharp precrack. Since $\eta b = (K_{IO}'/K_{IO})^2$ (Ref. 22), the bluntness parameter is about $(2.74)^2$ or 7.5. From the experimental data for a plate with similar width (120 mm) and heat input (3894 cal/cm or 16.3 kJ/cm) obtained by Tatsukawa and Oda (Ref. 24), the half width of the tension zone was found to be between 20 and 25 mm for different residual stress measuring methods. Hence, we used c = 22.5 mm in our simulation.

Using the parameters obtained above and solving Equation 2 numerically, the instantaneous crack length and speed were obtained. These were then substituted into Equation 1 to obtain the vertical surface displacement in the time domain at the epicenter as shown in Fig. 11A. The vertical velocity and acceleration are illustrated in Fig. 11B and C for comparison. The initial waveforms for vertical displacement, velocity, and acceleration are depicted in Fig. 12. Figure 13 gives the experimental initial motion within a period of 3.8 μs. Here, 3.8 μs is the time it takes for the P wave to arrive from secondary reflection. Comparing Figs. 11 and 12, the waveform of experimental result appears to be closer to that of the theoretical vertical displacement. The theoretical curve in Fig. 12A appears to be a superposition of a step function and a ramp function. The step function, however, can barely be observed in the experimental result given by Fig. 13. This is due to the fact that the AE sensor employed is a resonant transducer, which cannot respond well to high-frequency signals, as evident in Fig. 7B. As a result, the initial AE response is still largely influenced by the instrumentation.

The normalized theoretical spectra of the vertical displacement, velocity, and acceleration shown in Fig. 11 are depicted in Fig. 14. These can be compared with the experimental result in Fig. 10. We found that the experimental spec-

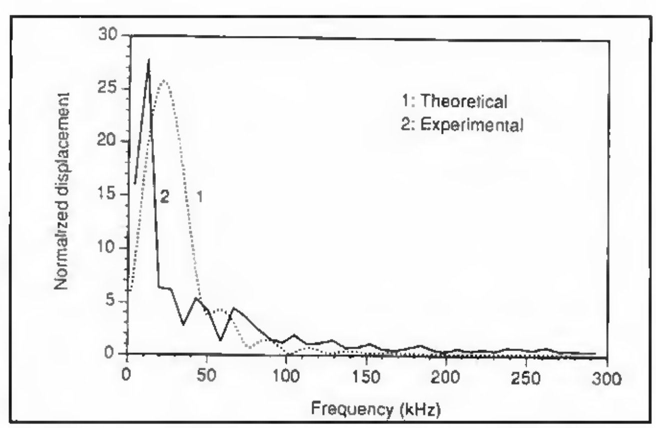

Fig. 15 — Comparison of theoretical and experimental spectra.

trum is closer to the theoretical spectrum of vertical displacement for this particular transducer. This is consistent with the observation in the time domain and the conclusion drawn earlier from the sensitivity charts in Fig. 3. Figure 14 shows the comparison of the spectrum from the experimental AE signals and that from the theoretical prediction of surface displacement. The envelopes for both spectra decrease with an increase in frequency. The fluctuations on each curve diminish at high frequencies. Reasonable consistency is observed. Note that the simulation only took into account the first motion of the P wave (Ref. 14), while the experimental result was for the surface motion from both P and S waves. This difference was responsible for the minor discrepancy between the experimental data and theoretical prediction. Furthermore, in the study of the relationship between AE and vibration characteristics of cast iron, Honjoh, *et al.* (Ref. 13), observed a reduction in the resonant frequency and increase in attenuation constant of the structure with crack extension. This indicates that the system transfer function utilized for deconvolution should vary with instantaneous crack length. However, because of the difficulty of calibrating the system during crack growth, we only calibrated the system before the propagation of the initial crack. This approximated transfer function might also contribute to the discrepancy in the frequencies corresponding to peaks in the magnitude in the experimental and simulated spectra. However, the overall results show reasonable consistency.

Conclusions

The AE signal generated by the propagation of a finite crack subject to nonuniform residual stress was recorded and analyzed in both time and frequency domains. The contamination of structure and instrumentation characteristics has been removed by deconvolution in the frequency domain, and its spectrum was compared with theoretical simulation. The experimental result was found to be closer to the surface displacement in both time and frequency domains. In the frequency domain, most of the high amplitude components are found to be clustered at frequencies below 200 kHz, while the high-frequency components are relatively small in amplitude. The envelopes for both experimental and theoretical spectra decrease with an increase in frequency, and the fluctuations in each curve diminish at high frequencies.

References

1. Liptai, R. G., and Tatro, C. A. 1976. Acoustic emission inspection. *Metals Handbook*, 8th ed., Vol. 11, pp. 234–243.

2. Tse, M.-K., Lincoln, M. A. W., and Gu, P.-Y. 1987. Real-time monitoring of the solidification rate in investment casting by thermography. Sensors for Manufacturing. The Winter Annual Meeting of the ASME, M.-K. Tse and D. Dornfeld, eds. pp. 121–138.

3. Purvis, A. L., Kannatey-Asibu, E., Jr., and Pehlke, R. D. 1990. Evaluation of acoustic emission from sand cast aluminum Alloy 319 during solidification and formation of casting defects. *AFS Transactions*, Vol. 98, pp. 1–7.

4. Dornfeld, D. A. 1991. Monitoring of the machining process by means of acoustic emission sensors. *Acoustic Emission: Current Practice and Future Directions*, ASTM STP 1077. Sachse, W., Roget, J., and Yamaguchi, K., eds., American Society for Testing and Materials, Philadelphia, pp. 328–344.

5. Dornfeld, D. A., and Kannatey-Asibu, E., Jr., . 1980. Acoustic emission during orthogonal metal cutting. *International Journal of Mechanical Sciences*, Vol. 22, pp. 285–296.

6. Liu, X., and Kannatey-Asibu, E.,Jr.,. 1990. Classification of AE signals for monitoring martensite formation from welding. *Welding Journal* 69(10): 389-s to 394-s.

7. Hartbower, C. E., Reuter, W. G., Morais, C. F., and Crimmins, P. P. 1972. Use of acoustic emission for the detection of weld and stress corrosion cracking. *Acoustic Emission*, ASTM STP 505. Philadelphia, pp. 187–221.

8. Romrell, D. M., 1973. Acoustic emission weld monitoring of nuclear components. *Welding Journal* 52(2): 81-s to 87-s.

9. Fikkers, A. T., 1974. Influence of external restraint on cold cracking. *Metal Construction and British Welding Journal*, Vol. 6, pp. 188–193.

10. Racko, D. 1987. Acoustic emission from welds as indicator of cracking. *Materials Science and Technology*, December, Vol. 3, pp. 1062–1066.

11. Graham, L. J., and Alers, G. A. 1974. Spectrum analysis of acoustic emission in A533-B steel. *Materials Evaluation*, Vol. 32, pp. 31–37.

12. Ono, K., and Ucisik, J. 1976. Acoustic emission behavior of aluminum alloys. *Materials Evaluation* 34(2): 32–44.

13. Honjoh, K., Sudoh, Y., and Masuda, J. 1986. Relationship between acoustic emission and vibration characteristics during destruction of cast iron. *Progress in Acoustic Emission III*, The Japanese Society of NDI, pp. 73–86.

14. Fang, C.-K., Kannatey-Asibu, E., Jr., and Barber, J. R. 1993. Far-field initial response of acoustic emission from cracking in a weldment. Submitted to *ASME Journal of Engineering for Industry*.

15. Kuo, S. 1987. Transformation-hardening materials: carbon and alloy steels. *Welding Metallurgy*, John Wiley & Sons, New York, pp. 319–366.

16. Spanner, J. C., Brown, A., Hay, D. R., Mustafa, V., Notvest, K., and Pollock, A. 1987. Fundamentals of acoustic emission testing. *Nondestructive Testing Handbook*, 2nd ed., Vol. 5, Sec. 1, pp. 11–44.

17. Ohira, T., Pao, Y. 1986. Microcrack initiation and acoustic emission during fracture toughness tests of A533B Steel. *Metallurgical Transactions A*, Vol. 17A, pp. 843–852.

18. Ohira, T., and Kishi. T., 1986. Effect of iron content on fracture toughness and cracking processes in high-strength Al-Zn-Mg-Cu alloy. *Materials Science and Engineering*, Vol. 78, pp. 9–19.

19. Sachse, W., and Hsu, N. N., 1979. Ultrasonic transducers for materials testing and their characterization. *Physical Acoustics: Principles and Methods*, W. P. Mason, and R. N. Thurston, eds., Academic Press, New York, Vol. XIV, pp. 277–405.

20. Kishi. T., and Ohira, T. 1983. Dynamic crack growth during pop-in fracture in 7075 aluminum alloy. *Transactions of the Japan Institute of Metals*, 24(4): 255–263.

21. Hsu, N. N., Simmons, J. A., and Hardy, S. C. 1977. An approach to acoustic emission signal analysis — theory and experiment. *Materials Evaluation* 35(10): 100–106.

22. Fang, C.-K., Kannatey-Asibu, E., Jr., and Barber, J. R. 1993 Crack-tip equation of motion due to nonuniform residual stresses in a weldment. Submitted to *ASME Journal of Engineering for Industry*.

23. Datta, K. P. 1981. Sharp crack and blunt notch toughness behavior of quenched and tempered AISI 4340 Steel. *Materials Science and Engineering*, Vol. 51, pp. 241–252.

24. Tatsukawa, I., and Oda, I. 1972. Distortions and residual stresses in arc welding. *Transactions of the Japan Welding Society* 3(2): 37–46.